

## CHAPTER 32

### Large-angle Parabolic Equation Methods

James T. Kirby\*

Large-angle parabolic equation methods for the propagation of surface water waves are discussed. The methods described here are limited to forms which are solvable by the Crank-Nicolson method, but are successful in opening the allowed range of propagation directions to  $\sim 50^\circ$  with respect to normal incidence.

#### Introduction

The application of the parabolic equation method (PEM) to any relevant wave propagation problem implies that a principal propagation direction may be identified in the  $\{x,y\}$  plane of propagation. Then, an aperture, or window of directions with respect to the principal direction, is associated with any particular approximation, and limits the range of propagation directions which may be adequately represented by the approximation (Figure 1). The borders of a given aperture are defined only loosely and depend mainly on the amount of error the modeller is willing to allow in the wave prediction. This error may be evaluated for any given approximation by examining the approximation in terms of the related expansion of the wavenumber vector. Errors in predicted wavelengths and propagation directions may then be evaluated directly.

The purpose of this paper is to examine two methods of extending the basic parabolic equation method to include large-angle effects. The first scheme is based on the Padé approximant extension of the lowest-order scheme, following the work of Booij (1981) and Dingemans (1983). The second scheme is based on a minimax principle, and has been applied previously by Green (1984) to the problem of underwater sound propagation.

#### Parabolic Equations and Padé Approximants

The lowest-order parabolic equation for forward scattering of time-harmonic linear waves in the  $x$  (principal) direction in water of constant depth may be derived by substituting

$$\eta(x,y) = A(x,y)e^{i(kx-\omega t)} \quad (1)$$

into the governing Helmholtz equation to obtain

$$2ikA_x + A_{yy} = 0 + \text{higher order terms} \quad (2)$$

\*Assistant Professor, Coastal and Oceanographic Engineering Department, University of Florida, Gainesville, FL 32611

where we have assumed that  $|A_x| \ll 0(k|A|)$ . This approximation may be examined in light of the plane wave of permanent form

$$\eta = ae^{i(\ell x + my - \omega t)} \quad ; \quad \ell^2 + m^2 = k^2 \tag{3}$$

$A(x,y)$  in eq. (1) is then given by

$$A(x,y) = ae^{i[(\ell-k)x + my]} \tag{4}$$

which gives

$$\frac{\ell}{k} = 1 - \frac{1}{2} \left(\frac{m}{k}\right)^2 \tag{5}$$

after substitution in eq. (2). Equation (5) in turn is the lowest order binomial expansion of

$$\frac{\ell}{k} = \left\{ 1 - \left(\frac{m}{k}\right)^2 \right\}^{1/2} \tag{6}$$

for fixed  $m/k = \sin\theta \ll 1$ ,  $\theta$  being the propagation direction. The accuracy of any approximation over the range of propagation directions  $0 < \theta < \theta_a$ , where  $\theta_a$  is the aperture width, may be evaluated by comparing predicted  $\ell/k$  to exact  $\ell/k = \cos\theta$  over the range in question. This comparison is given in Figure 2 for eq. (5). Equation (5) forms the basis of the so-called lowest-order approximation.

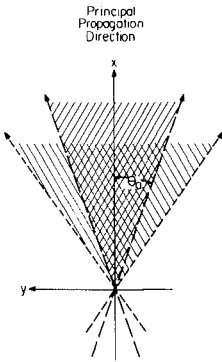


Fig. 1: Definition of aperture for parabolic approximations  
 //// allowed aperture: lower-order approximation  
 \\\\ allowed aperture: higher-order approximation (reprinted with permission of Elsevier Press)

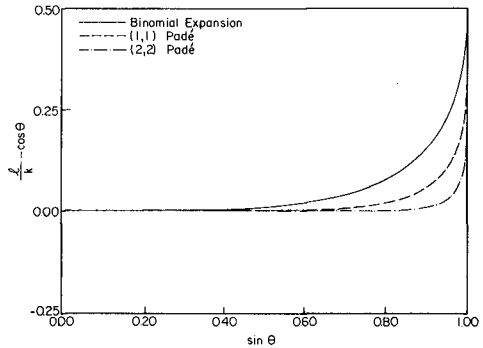


Fig. 2: Absolute errors  $(\ell/k) - \cos\theta$  for several expansions of  $(\ell/k) = (1 - (m/k)^2)^{1/2}$  about  $(m/k) \rightarrow 0$  (reprinted with permission of Elsevier Press)

One of the simplest ways of extending the accuracy of a polynomial expansion is to construct a rational approximation consisting of the ratio of two polynomial expressions. Of the possible choices, the Padé approximant serves as the logical starting point (Baker, 1975). For eq. (6), the appropriate (1,1) Padé approximant is given by

$$\left(\frac{\ell}{k}\right) = \frac{1 - \frac{3}{4} \left(\frac{m}{k}\right)^2}{1 - \frac{1}{4} \left(\frac{m}{k}\right)^2} \quad (7)$$

The Padé approximant has the property of predicting the proper value and slope of the approximated function  $\ell/k$  as  $m/k$  (or  $\theta$ ) becomes small. The approximation thus maintains the accuracy of the lowest-order approximation at small  $\theta$ , and at the same time extends the accuracy of the approximation as  $\theta$  increases, as shown in Figure 2. Using eq. (7) and retracing the steps of eqs. (2-5) in reverse order then gives

$$2ikA_x + A_{yy} + \frac{1}{2k} A_{xyy} = 0 \quad (8)$$

Dingemans (1983) has shown that the no-current, constant depth form of Booijs's (1981) parabolic approximation is essentially equivalent to eq. (8), and proposed the Padé approximant as the relevant analysis of the splitting method employed by Booijs to obtain his PEM approximation.

#### Padé Approximant: Computational Example

As a test of the higher-order parabolic model, we study the wave field in the vicinity of the shore-attached breakwater described in Figure 3. An extensive set of data for the wave field in the shadow zone downwave of the breakwater has been given by Hales (1980) for a number of wave periods, amplitudes, and angles of incidence. A closed form asymptotic solution in the linear, mild-slope approximation has been provided by Liu *et al.* (1979) and has been compared to the experimental data by Liu (1982), who found qualitative agreement between the linear theory and experimental results.

The parabolic equation for the general case of uneven topography was developed according to the approximation of the previous section and is given in Kirby (1986).

For this case, we restrict our attention to the linearized theory in order to compare parabolic model results to the asymptotic theory of Liu *et al.* The experimental results are complicated by the presence of a wave-induced current system due to the surf zone in close proximity to the measurement transects, and it is likely that neglected wave-current interaction effects have as much influence on the data as the neglected nonlinearity.

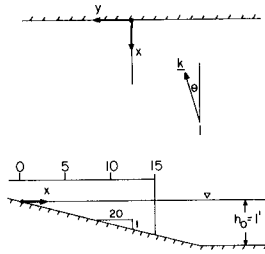


Fig. 3: Geometry of shore-attached breakwater (reprinted with permission of AGU)

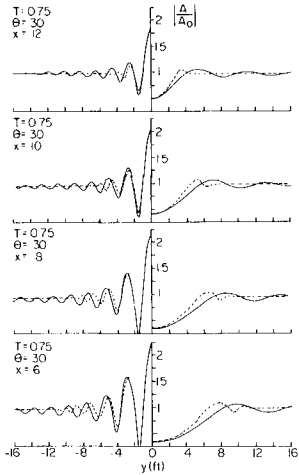


Fig. 4a: Shore-attached breakwater: comparison of lowest-order approximation and asymptotic theory of Liu et al (1979). Dashed line, lowest-order approximation; solid line, asymptotic theory;  $T = 0.75$  s,  $\theta = 30^\circ$ . (reprinted with permission of AGU)

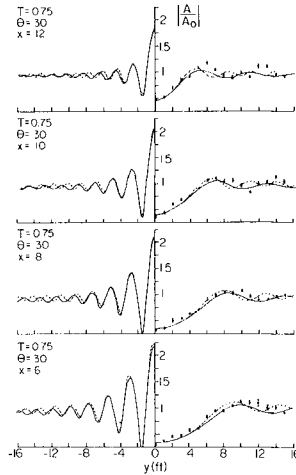


Fig. 4b: Shore-attached breakwater: comparison of higher-order approximation, asymptotic theory of Liu et al (1979), and data of Hales (1980). Dashed line, higher-order approximation; solid line, asymptotic theory,  $\phi$  experimental data;  $T = 0.75$  s,  $\theta = 30^\circ$ . (reprinted with permission of AGU)

The geometry corresponding to the experimental arrangement consists of a plane beach with slope 1:20, extending out to a depth of 1 ft (.3048 m), beyond which the bottom is flat. The x coordinate is oriented offshore from the shoreline. The breakwater extends to  $x = 15$  ft (4.572 m), and measured wave data in the shadow zone of the breakwater are available for the transects  $x = 6, 8, 10,$  and  $12$  ft (1.829, 2.438, 3.048, and 3.658 m) (Hales, 1980). Values for incident wave data are with reference to the offshore region with  $h = 1$  ft (.3048 m).

In Figures 4a and 5a we show comparisons of the predictions of the lowest-order approximation with the asymptotic theory of Liu *et al* for the extremes of the test conditions  $T = 0.75$  s,  $\theta = 30^\circ$  and  $T = 1.5$  s,  $\theta = 20^\circ$ , respectively. In both cases it is apparent that the diffracted wave disturbance spreads laterally at a much slower rate in the lower-order approximation than in the analytic theory, which encompasses an unapproximated mild-slope equation. Both the height of the reflected wave on the upwave side of the breakwater and the wave height in the shadow zone adjacent to the downwave side of the breakwater are well predicted. However, most of the diffracted wave information is lost farther from the breakwater, well before significant amplitude modulations in the asymptotic wave field die out. These results indicate that the group velocity for lateral motion of diffracted waves is too small in the lower-order approximation.

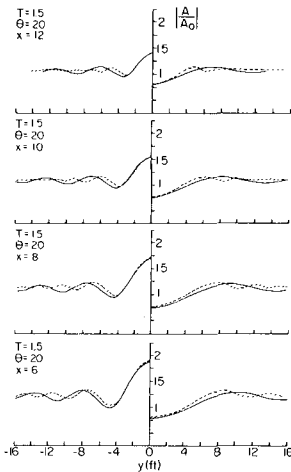


Fig. 5a: As in Figure 4a;  $T = 1.5$  s,  $\theta = 20^\circ$ . (reprinted with permission of AGU)

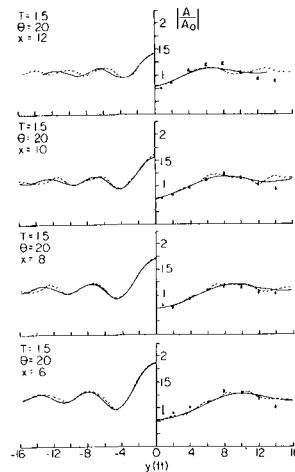


Fig. 5b: As in Figure 4b;  $T = 1.5$  s,  $\theta = 20^\circ$ . (reprinted with permission of AGU)

For the Padé approximation, plots of results for the two test conditions are given in Figures 4b and 5b. Data in the shadow and downwave regions for these cases correspond to the lowest-amplitude runs from Hales (1980), which would be expected to correspond more

closely to the assumption of linearity. The plots indicate that the diffracted wave field is able to spread laterally in the higher-order approximation to a much greater degree than in the lower-order approximation. A comparison of the parabolic model results to the asymptotic theory indicates that the parabolic model is initially contaminated by components with large transverse wavenumber, which cause the computed amplitude modulations transverse to the breakwater to undulate more rapidly than the corresponding asymptotic results. These rapid undulations may be successfully damped using any one of several types of dissipative filters.

### Minimax Approximation

Greene (1984) has suggested that improvements may be achieved while staying within the scheme of eq. (7) by relaxing the exact connection between eq. (7) and eq. (6) as  $(m/k) \rightarrow 0$  in favor of adopting an approximation which minimizes the maximum error  $(\ell/k - \cos\theta)$  over a prespecified aperture  $0 < \theta < \theta_a$ . These so-called minimax approximations may be written in the present context as

$$\left(\frac{\ell}{k}\right) = \frac{a_0 + a_1 \left(\frac{m}{k}\right)^2}{1 + b_1 \left(\frac{m}{k}\right)}, \quad (9)$$

The coefficients of the minimax approximation are chosen so as to minimize the error

$$e = \text{MAX}|\ell/k(\theta) - \cos\theta| \quad ; \quad 0 < \theta < \theta_a, \quad \theta_a \text{ given} \quad (10)$$

where  $\ell/k$  is predicted by eq. (12) and  $\cos\theta = \ell/k$  is given by eq. (6). The procedure for obtaining minimax approximations is too extensive to summarize here; the reader is referred, for example, to Chapter 6 of Morris (1983). A list of values of  $a_0$ ,  $a_1$  and  $b_1$  are given in Table 1 for aperture widths ranging from  $10^\circ$  to  $90^\circ$  in increments of  $10^\circ$ . The coefficient values are seen to be asymptotic to the (1,1) Padé approximant at  $\theta_a \rightarrow 0$ . Figure 6 gives plots of the absolute error in predicted  $(\ell/k)$  for values of  $\theta_a = 40^\circ$ ,  $60^\circ$  and  $80^\circ$ . A plot of the (1,1) Padé approximant is included for comparison. For values of  $\theta_a < 60^\circ$ , the correspondence between the minimax and (1,1) Padé approximant remains close at  $\theta=0$ , the deviation for  $\theta_a = 60^\circ$  being  $(1 - a_0) \times 100 = 0.2\%$ . Deviations for  $\theta_a > 60^\circ$  at  $\theta=0$  increase rapidly due to the difficulty in approximating eq. (7) as  $m/k \rightarrow 1$ . However, the advantages of the  $\theta_a = 60^\circ$  approximation over the (1,1) Padé approximant, when considered over the entire range  $0 < m/k < 1$ , are apparent. A comparison of Figures 2 and 6 indicates that the  $\theta_a = 60^\circ$  approximation attains about the same level of accuracy as  $m/k \rightarrow 1$  as the (2,2) Padé approximant, with only a slight decrease in accuracy at small values of  $\theta$ .

Equation (12) may be used to derive the corresponding parabolic approximation

TABLE 1. COEFFICIENTS OF THE RATIONAL APPROXIMATION DETERMINED BY VARYING APERTURE WIDTH.

Aperture	$a_0$	$a_1$	$b_1$
Padé	1	-.75	-.25
10°	.999999972	-.752858477	-.252874920
20°	.999998178	-.761464683	-.261734267
30°	.999978391	-.775898646	-.277321130
40°	.999871128	-.796244743	-.301017258
50°	.999465861	-.822482968	-.335107575
60°	.998213736	-.854229482	-.383283081
70°	.994733030	-.890064831	-.451640568
80°	.985273164	-.925464479	-.550974375
90°	.956311082	-.943396628	-.704401903

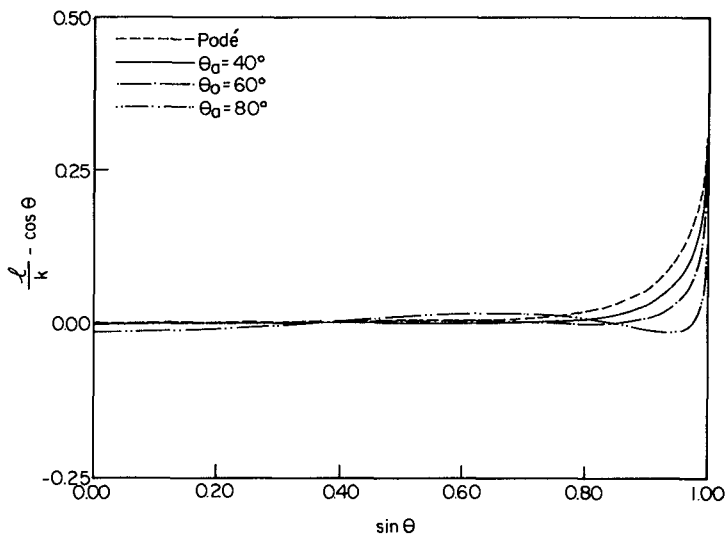


Fig. 6: Absolute errors  $(l/k) - \cos \theta$  for various aperture widths  $\theta_a$  for the minimax (1,1) rational approximation. (reprinted with permission of Elsevier Press)

$$2ika_x + 2k^2(a_0 - 1)A + 2(b_1 - a_1)A_{yy} - \frac{2ib_1}{k} A_{xyy} = 0 \quad (11)$$

which reduces to eq. (10) as  $\theta_a \rightarrow 0$ .

### Tests of the Minimax Approximation at Large Angles of Incidence

The minimax approximation of the previous section has been used to develop a corresponding refraction-diffraction model including the effects of weak nonlinearity and wave current interaction; details are given in Kirby (1987). In order to test the large-angle capabilities of the model, we choose a shoal geometry given by

$$h(x,y) = \begin{cases} h_0 = 0.336 \text{ m} & ; \quad r > R \\ h_0 + 0.3 - 0.5 \left\{ 1 - \left[ \left( \frac{x}{5} \right)^2 + \left( \frac{y}{5} \right)^2 \right] \right\}^{1/2} & ; \quad r < R \end{cases}$$

where  $R = 4$  m and  $r = (x^2 + y^2)^{1/2}$ . The symmetry of the shoal allows the incident wave field to be rotated to any angle to the x-axis; a "correct" model will be one that causes no distortion to the resulting focusing pattern resulting from changes in  $\theta_0$ , the incidence angle.

We take a rectangular grid with  $\Delta x' = \Delta y' = 0.25$  m and overall dimensions  $0 < x'y' < 24.75$  m. We use the incident wave period and amplitude conditions of Berkhoff *et al* (1982). Two incident wave directions are studied;  $\theta_0 = 0^\circ$ , with the shoal centered at  $(x',y') = (5,10)$ , and  $\theta_0 = 45^\circ$ , with the shoal centered at  $(x',y') = (5,5)$ .

For the first series of tests, we use the (1,1) Padé model to study the two incident wave angles. Figure 7 shows the wave patterns for the two incidence angles in the form of contours of surface elevation in increments of  $0.5 A_0$ . The asymmetrical distortion to the focusing pattern at the  $45^\circ$  angle of incidence is apparent, as is a tendency for the focus to be shifted off the picture diagonal in the +x direction, or downwave in the computational sense. The distortion to the wave pattern due to the  $45^\circ$  angle of incidence is illustrated clearly by the superposition of wave amplitude contours in Figure 8. The superposition was obtained by rotating the wave field of Figure 7b about the center of the shoal by  $36.5^\circ$  in a counterclockwise sense, or  $45^\circ$  minus an  $8.5^\circ$  distortion which represents the angle between the diagonal and the line joining the shoal center to the point of maximum wave height in the focus. This  $8.5^\circ$  distortion accounts for the shift of the diffraction pattern in the downwave sense on the computation grid. Figure 8 shows clearly that the focus is elongated and shifted further from the shoal center than in the normal incidence case, with corresponding distortion in the diffraction fringes. Contour values in Figure 8 (and 10) are relative to incident wave amplitude.

Figure 9 shows the wave field for the  $45^\circ$  angle of incidence, using the  $\theta_a = 70^\circ$  minimax approximation. There is still some apparent asymmetric distortion and a shift of the focus off the diagonal in the +x direction; however, these effects are much less accentuated

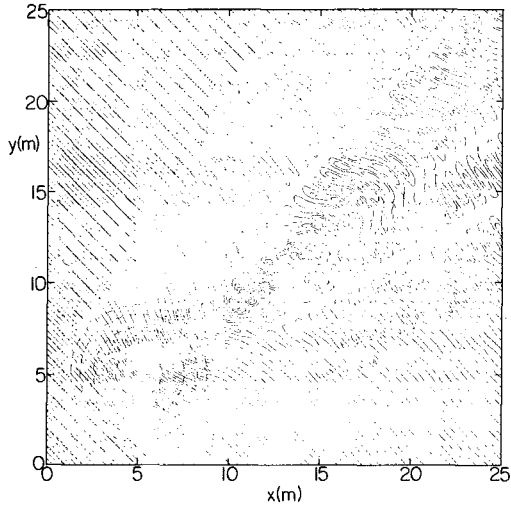
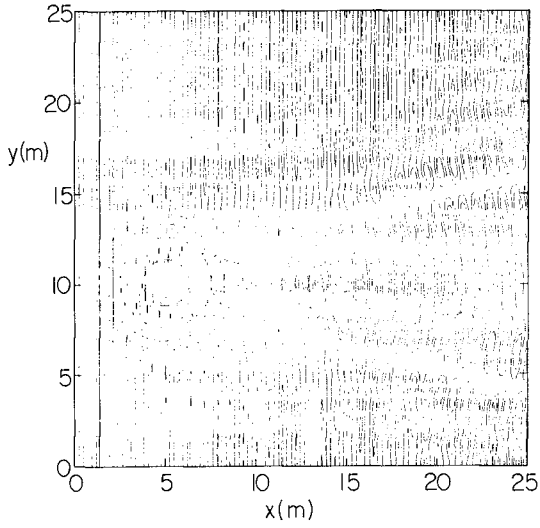


Fig. 7: Wave fields calculated using the (1,1) Padé model. Contours are in increments of  $0.5 A_0$  for instantaneous  $\eta(x,y)$ . a)  $\theta_0 = 0$ , normal incidence. b)  $\theta_0 = 45^\circ$ . (reprinted with permission of Elsevier Press)

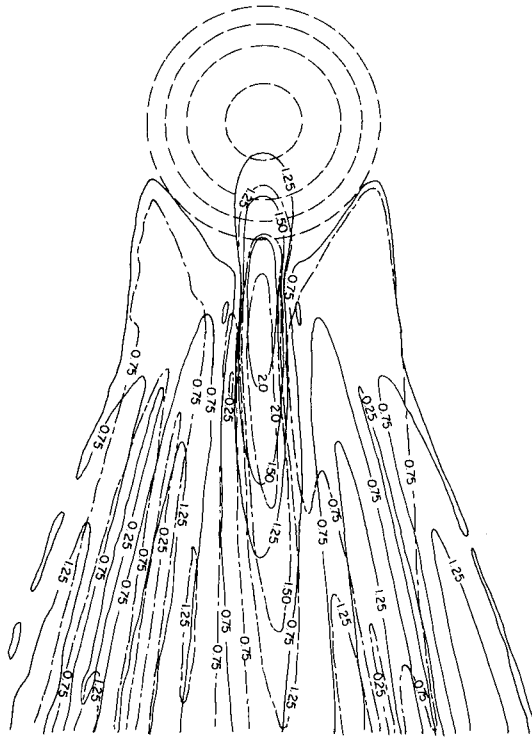


Fig. 8: Amplitude contours and topography for circular shoal. Amplitude contours  $|A/A_0|$  as labelled; (1,1) Padé approximant. —  $\theta_0 = 0^\circ$ ; -.-  $\theta_0 = 45^\circ$ ; --- depth contours. (reprinted with permission of Elsevier Press)

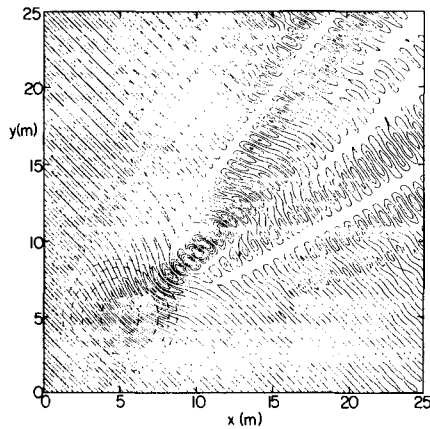


Fig. 9: Wave field calculated using  $\theta_a = 70^\circ$  model;  $\theta_0 = 45^\circ$ . Contours as in Figure 7. (reprinted with permission of Elsevier Press)



Refraction Effects in Parabolic Approximations

For the special case of topographies varying as  $h(x)$  only, and for angles of incidence  $\theta_0$  at reference depth  $h_0$ , each of the parabolic approximations may be solved to yield an estimate of the leading-order, slowly varying wave field undergoing shoaling and refraction. Solutions for the full refraction approximation and for each of three parabolic methods follow:

Exact Refraction Solution

$$\eta = A_0 \left( \frac{C_{g_0}}{C_g} \right)^{1/2} \left( \frac{\cos \theta_0}{\cos \theta} \right)^{1/2} e^{i \int k \cos \theta \, dx - my} \quad (12)$$

Small-Angle Equation Solution

$$\eta = A_0 \left( \frac{C_{g_0}}{C_g} \right)^{1/2} e^{i \int k \left( \frac{\ell}{k} \right) dx - my} ; \frac{\ell}{k} = 1 - \frac{1}{2} \left( \frac{m}{k} \right)^2 \quad (13)$$

(1,1) Padé Approximation

$$\eta = A_0 \left( \frac{C_{g_0}}{C_g} \right)^{1/2} \frac{(1 - \frac{1}{4} \sin^2 \theta_0)}{(1 - \frac{1}{4} \sin^2 \theta)} e^{i \int k \left( \frac{\ell}{k} \right) dx - my} ; \frac{\ell}{k} = \frac{1 - \frac{3}{4} \left( \frac{m}{k} \right)^2}{1 - \frac{1}{4} \left( \frac{m}{k} \right)^2} \quad (14)$$

Minimax Approximation

$$\eta = A_0 \left( \frac{C_{g_0}}{C_g} \right)^{1/2} \frac{(1 + b_1 \sin^2 \theta_0)}{(1 + b_1 \sin^2 \theta)} e^{i \int k \left( \frac{\ell}{k} \right) dx - my} ; \frac{\ell}{k} = \frac{a_0 + a_1 \left( \frac{m}{k} \right)^2}{1 + b_1 \left( \frac{m}{k} \right)^2} \quad (15)$$

It is apparent that, with each increase in level of approximation, that the phase function of the shoaled wave becomes better approximated. Also apparent are large variations in each model's ability to reproduce the refraction coefficient  $(\cos \theta_0 / \cos \theta)^{1/2}$  of the "exact" solution; in particular, it is not modelled at all in the lowest-order case and is only apparent starting with the (1,1) Padé approximant method. Figure 11 gives results for computed refraction coefficients for four angles of incidence  $20^\circ$ ,  $40^\circ$ ,  $60^\circ$ , and  $80^\circ$  with respect to shore-normal. The minimax values are based on a chosen

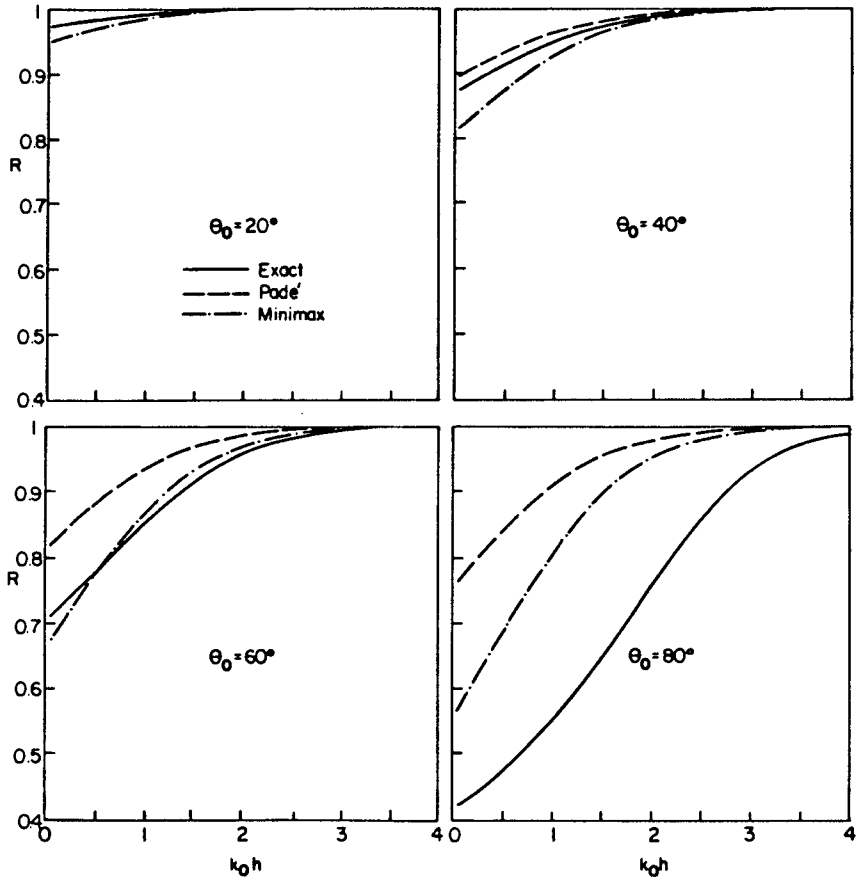


Fig. 11: Variation in refraction coefficient with deepwater angle of incidence  $\theta_0$  and water depth.

width  $\theta_a = 70^\circ$ . For small angles of incidence, the (1,1) Padé approximant method exhibits favorable behavior in comparison to the minimax approximation, due to its enhanced level of accuracy as local  $\theta(x) \rightarrow 0$ . However, for  $\theta_0 = 60^\circ$ , the minimax approximation performs quite well, while the (1,1) Padé approximant is clearly over-extended. For  $\theta_0 = 80^\circ$ , the propagation angle is outside the range of both higher-order models, and each perform poorly. In each of the cases above,  $\theta_0$  is taken to be the deepwater value.

### Conclusions

It has been shown that the range of wave angles which is allowable within the limitations of the parabolic approximation may be significantly increased by relaxing the local accuracy of approximations based on Padé approximants at normal wave incidence in favor of minimax approximations, which minimize the maximum error occurring over a prespecified range of wave directions. We have shown that the minimax approximations provide quantitatively accurate results for a focussing pattern developing in a wave propagating at  $45^\circ$  to the principal direction. This range of quantitative accuracy is seen to be well beyond the limitations of the (1,1) Padé approximant model given above. Results for wave refraction calculations suggest that it would be desirable to limit the aperture width  $\theta_a$  in the minimax approximation to a value consistent with the largest expected local propagation direction, since the Padé approximant model is somewhat better at predicting the refraction coefficient at small angles of incidence.

### References

- Baker, G.A., 1975, Essentials of Padé Approximants, Academic Press.
- Berkhoff, J.C.W., Booij, N, and Radder, A.C., 1982, "Verification of numerical wave propagation models for simple harmonic linear waves", Coastal Eng. 6, 255-279.
- Booij, N., 1981, "Gravity waves on water with non-uniform depth and current", Report 81-1, Dept. of Civil Eng., Delft Univ. of Technology.
- Dingemans, M.W., 1983, "Verification of numerical wave propagation models with field measurements: CREDIZ verification Haringvliet", Report W488 part 1, Delft Hydraulics Laboratory.
- Greene, R.R., 1984, "The rational approximation to the acoustic wave equation with bottom interaction", J. Acoust. Soc. Am., 76, 1764-1733.
- Hales, L.Z., 1980, "Erosion control of scour during construction, report 3, Experimental measurements of refraction, diffraction, and current patterns near jetties", Tech. Rep. HL-80-3, U.S. Army Eng. Waterways Exp. Stn., Vicksburg, Ms.

- Kirby, J.T., 1986, "Higher-order approximations in the parabolic equation method for water waves", J. Geophys. Res., 91, 933-952.
- Kirby, J.T., 1987, "Rational approximations in the parabolic equation method for water waves", Coastal Engineering, in press.
- Liu, P.L.-F., 1982, "Combined refraction and diffraction: comparison between theory and experiments," J. Geophys. Res. 87, 5723-5730.
- Liu, P.L.-F., Lozano, C.J., and Pantazaras, N., 1979, "An asymptotic theory of combined wave refraction and diffraction", Appl. Ocean Res., 1, 137-146,.
- Morris, J.Ll., 1983, Computational Methods in Elementary Numerical Analysis, John Wiley and Sons.